

# Patch-Clamp Studies of Voltage-Gated Currents in Identified Neurons of the Rat Cerebral Cortex

O. P. Hamill, J. R. Huguenard, and  
D. A. Prince

Department of Neurology, Stanford University  
School of Medicine, Stanford, California

**In the cerebral cortex, neurons can be classified into 2 broad morphological classes, referred to as pyramidal and nonpyramidal (stellate) cells, which correspond to functional classes of projection neurons and local circuit interneurons, respectively. In this study, we demonstrate that specific morphological, immunohistochemical, and physiological features, that allow class distinction of neurons *in situ*, are retained in acutely isolated neocortical neurons. Furthermore, voltage-clamp analysis with patch-clamp techniques indicate the differences in functional properties in adult neurons, reflect cell-specific, developmental changes in the density and type of specific classes of Na<sup>+</sup>, K<sup>+</sup> and Ca<sup>2+</sup> channels expressed. The differences in channel properties contribute to the different input-output relations of neocortical neurons, which enable inhibitory neurons to follow excitatory inputs faithfully and projection neurons to have more integrative roles.**

In the cerebral cortex, specific classes of neurons can be recognized by their morphology and histochemistry (for reviews see Peters and Jones, 1984; Schmitt et al., 1985). Furthermore, because of the distinctive horizontal lamination of neuronal cell bodies and their modality-specific vertical arrangement in columns, they can be classified by neuronal position (Mountcastle, 1957; Hubel and Wiesel, 1962). In order to understand the specific role played by neural elements in information processing by local neural circuits, physiological variations between specific neuronal types must also be identified. Recognition of functional differences within morphological cell types in the cerebral cortex was first made possible by recording from identified neurons labelled by intracellular injection of dyes (Kelly and Van Essen, 1974; Gilbert and Wiesel, 1979). More recently, studies using this technique on brain slice preparations have shown that neocortical neurons belonging to the major morphological classes, pyramidal and aspiny stellate, can be further distinguished by differences in their action potential (AP) shape and repetitive firing properties in response to stimulation with constant current pulses (McCormick et al., 1985).

This study is concerned with the possible membrane channel mechanisms that may underlie the differences in firing properties observed previously in brain slice recordings (McCormick et al., 1985). We have used standard patch-clamp techniques to study neurons of the cerebral cortex acutely isolated from rats at well defined stages of development. We have also addressed the question of which developmental stage first evidences cell-type specific differences. This study focuses on some, but not all, of the well known classes of voltage-gated Na<sup>+</sup>, K<sup>+</sup> and Ca<sup>2+</sup> channels that have been described previously in invertebrate and vertebrate neurons (Adams et al., 1980; Adams and Galvan, 1984).

## Materials and Methods

### *Acute Isolation of Neocortical Neurons*

Dissociation of neocortical neurons was carried out according to the procedures described previously for guinea pig hippocampal neurons (Kay and Wong, 1986). The modified procedure, as we used it on the rat cerebral cortex, is briefly outlined below. The rat was first guillotined and the brain removed, taking

care to keep the brain cold during dissection by periodically dousing it with cold saline. One hemisphere was then mounted with "crazy glue" on a vibraslice chuck. At the slowest speed and highest amplitude, two to three 600-micron slices were made through the sensorimotor cortex. Then on a bed of ice, the cortex was dissected away from the rest of the brain structures using forceps and scalpel blade, attempting to remove the pia and most of the white matter. Using a scalpel blade, the remaining cortex was cut into 1-mm chunks. Approximately 8 chunks were then placed in the dissociation chamber using a wide bore (2 mm), fire polished pipette. The chamber contained normal physiological saline (in mM: 130 NaCl, 5 KCl, 1 CaCl<sub>2</sub>, 1 MgCl<sub>2</sub>, 25 dextrose, 20 HEPES buffer, bubbled with carbogen to give a pH of 7.0) and 2 mg/ml papain (Sigma Type IV) preactivated with cysteine. In this solution the chunks were kept suspended by gently stirring with a small stir bar. Depending on the developmental age, the chunks were removed after 45–90 min incubation (28°C) (i.e., at younger ages the incubation time was shorter) and transferred to a trituration vial containing 5 ml of saline. The partially digested chunks were then gently triturated with fire polished pipettes of progressively smaller bores. Following the final trituration the cells were passed through a 200- $\mu$ m nylon sieve to remove debris, into 35-mm culture dishes. The cells were then allowed to settle 30–60 minutes in oxygenated saline before recording procedures commenced.

Following the above procedure approximately 50% to 90% of cells retained processes, some as long as 1 mm. As a general rule the neurons with the most intact processes could be obtained from dissociations in which trituration was minimal; the sieving was required to remove the undissociated chunks. To avoid space clamp problems we did not record from pyramidal neurons with the longest processes, but rather from those with relatively compact dendrites similar to the one illustrated in Figure 1B. The yield of healthy cells tended to decrease as the age of the animal increased, nevertheless it was possible to obtain recordings from animals as old as 55 days. For the youngest cells, we used embryos of ages E17 to E21 that had been delivered by cesarean section under pentobarbital (50 mg/kg) anesthesia.

#### ***Viability of Acutely Dissociated Neurons and Their Passive Electrical Properties***

In refining the dissociation procedure a number of passive electrical parameters were used to establish the viability of the cells. Acutely dissociated neurons that looked physically healthy had resting potentials (measured immediately after rupture of the patch for whole cell recording, see below) around  $-50$  mV, which is lower than the average of  $-70$  mV measured in cerebral cortical neurons in slices (McCormick et al., 1985). We believe the difference may reflect the partial loss of transmembrane ionic gradients during the dissociation procedure. Input resistances were in the range of 500–1500 M $\Omega$ , which is an order of magnitude higher than the reported input resistances of

neocortical neurons recorded in slices which range between 10 and 100 M $\Omega$  (McCormick et al., 1985). We believe the significantly higher values arise because dissociated neurons have their distal processes truncated and because tight-seal whole cell recording reduces the leakage conductance around the recording electrode. The high input resistance of dissociated neurons and reduced dendritic tree facilitates whole cell recording by reducing series resistance and space clamp errors, respectively. In contrast to the large differences in input resistances observed between the preparations, membrane time constant measurements indicated a range of 10–50 msec similar to that reported for neurons in brain slice measurements (McCormick et al., 1985). Since the major focus of our study was on active membrane properties per se we did not carry out a detailed analysis of the passive electrical properties as either a function of age or development.

#### ***Labeling of Neocortical Neurons in the Slice and Following Isolation***

Pyramidal cells in the slice were labeled for morphological study by retrograde uptake of horseradish peroxidase (HRP) that was microinjected into the white matter of the cortex (Mesulam, 1982). Neurons expressing the enzyme glutamic acid decarboxylase (GAD), the  $\gamma$ -aminobutyric acid (GABA) synthesizing enzyme, were labeled immunocytochemically using a sheep antiserum (code 1440) that was raised to rat brain and was kindly provided to us by Dr. Donald Schmechel, together with the labeling protocol modified for use with dissociated neurons. The immunohistochemical procedure we used to stain neurons in cortical slices was the same as described by Oertel et al. (1981; see also McCormick et al., 1985).

#### ***Electrophysiological Recording and Analysis of Data***

Recordings were obtained from isolated neurons using the whole cell clamp configuration (Hamill et al., 1981). Electrodes were pulled from thin-walled glass capillaries (W-P Instruments, TW-150), to have a tip opening of approximately 2  $\mu$ m. They were then Sylgard (Dow-Corning) coated and fire-polished. When filled with a typical saline solution (see Table 1) they had resistances of between 1 and 2 M $\Omega$ . A List model EPC-7 (List Instruments) patch-clamp amplifier was used, which allowed 90% series resistance compensation of the estimated patch electrode access resistance.

#### ***Isolation of Membrane Currents***

The specific salt solutions, extracellular (E) and intracellular (I), used in this study to isolate as well as maximize Na<sup>+</sup>, K<sup>+</sup>, and Ca<sup>2+</sup> currents, are listed in Table 1. In most cases, with one exception, the extracellular solution was perfused into the bath chamber (1 ml volume) at approximately 1 ml/min. In order to study Ca<sup>2+</sup> currents, solution E<sub>4</sub> was locally puffed onto the cell using a blunt micropipette, approximately 10- $\mu$ m tip diameter, while the bath was

**Table 1**

Solutions appropriate for recording action potentials and isolating specific membrane currents

Recording		NaCl	Cho- line Cl	KCl	CsF	KF	CaCl <sub>2</sub>	MgCl <sub>2</sub>	HEPES	EGTA	TTX	TEA Cl	Cd Cl <sub>2</sub>
Extracellular solutions													
E <sub>1</sub>	Action potentials	140	—	3	—	—	1	1	10(Na <sup>+</sup> )	—	—	—	—
E <sub>2</sub>	Na <sup>+</sup> currents	140	—	—	—	—	1	1	10(Na <sup>+</sup> )	—	—	—	0.5
E <sub>3</sub>	K <sup>+</sup> currents	140	—	3	—	—	1	1	10(Na <sup>+</sup> )	—	0.001	—	0.5
E <sub>4</sub>	Ca <sup>2+</sup> currents	—	110	—	—	—	15	—	10(Na <sup>+</sup> )	—	0.001	—	—
Intracellular solutions													
I <sub>1</sub>	Action potentials	—	—	130	—	—	1	1	10(K <sup>+</sup> )	11(K <sup>+</sup> )	—	—	—
I <sub>2</sub>	Na <sup>+</sup> currents	5	—	—	120	—	1	1	10(Cs <sup>+</sup> )	11(Cs <sup>+</sup> )	—	5	—
I <sub>3</sub>	K <sup>+</sup> currents	—	—	—	—	130	1	1	10(K <sup>+</sup> )	11(K <sup>+</sup> )	—	—	—
I <sub>4</sub>	Ca <sup>2+</sup> currents	—	120	—	—	—	1	1	10(Cs <sup>+</sup> )	11(Cs <sup>+</sup> )	—	—	—

All concentrations are in millimoles. HEPES was adjusted to pH 7.4 with NaOH, KOH or CsOH, as indicated. Osmolarity of the solutions was ~300 milliosmoles.

perfused with E<sub>1</sub>. We used an elevated Ca<sup>2+</sup> concentration of 15 mM in order to amplify the Ca<sup>2+</sup> current. Inclusion of an inert food dye in the Ca<sup>2+</sup> solution indicated that it flooded the immediate environment of the neuron. This procedure of localized perfusion was found to maintain the viability of the surrounding neurons. We used parameters describing Na<sup>+</sup>, as well as K<sup>+</sup> and Ca<sup>2+</sup>, currents that were derived from observations on 3–12 neurons of each cell type at the different developmental ages. Because the membrane surface area changes during development, the densities of conductances in different cells at different developmental stages were determined as a “normalized conductance density.” This measurement, which has the units pS/μm<sup>2</sup>, was calculated by measuring the slope conductance from current–voltage (I–V) relations and normalizing the value for membrane area that was estimated from the measured total cell capacitance (i.e., read directly off the C slow dial of the EPC-7), assuming 1 μF/cm<sup>2</sup>.

#### The Developmental Time Frame Studied

The choice of the developmental time frame was determined by the ability to recognize specific cell types. From autoradiographic studies it is known that all neocortical neurons are generated outside the cortex from neuroblasts lining the immature ventricular wall (Berry and Rogers, 1965; Hicks and D'Amato, 1968; Shimada and Langman, 1970). Because precursor cells and preneurons in the proliferative zone display a similar bipolar morphology and cannot be easily distinguished (Berry and Rogers, 1965), we have studied only identifiable postmitotic neurons that have already migrated into the cortical plate, beginning at embryonic stage E17. At this age, isolated cells with either stellate or pyramidal-like morphologies could be distinguished. Nonpyramidal and pyramidal cells

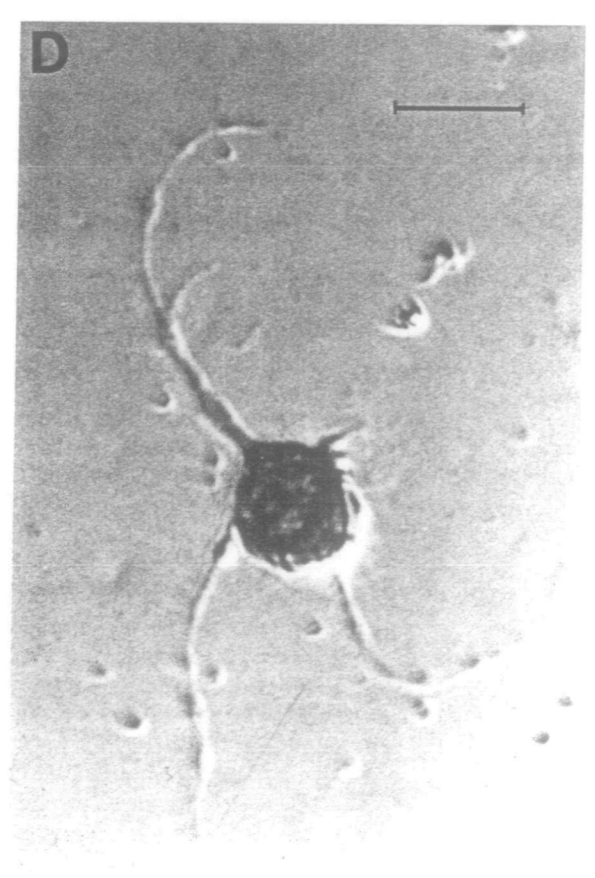
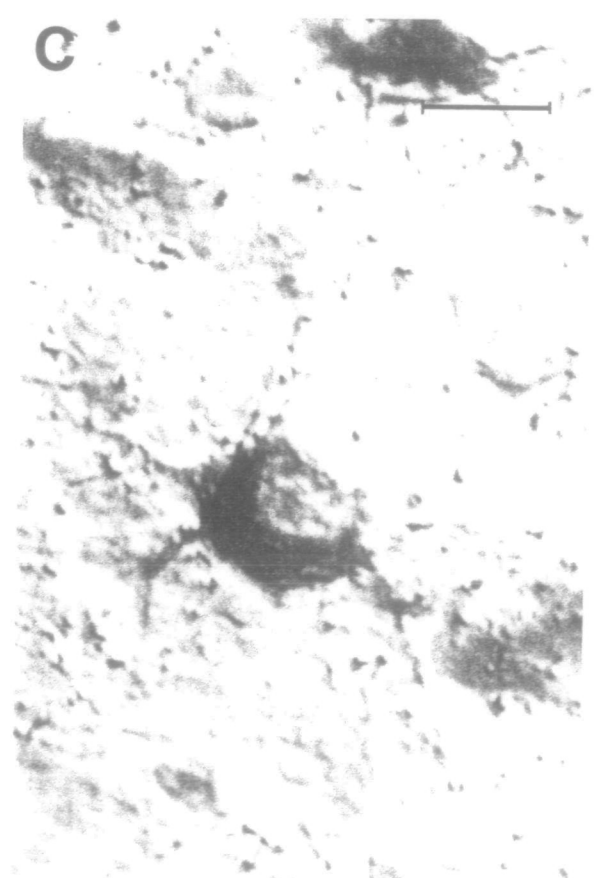
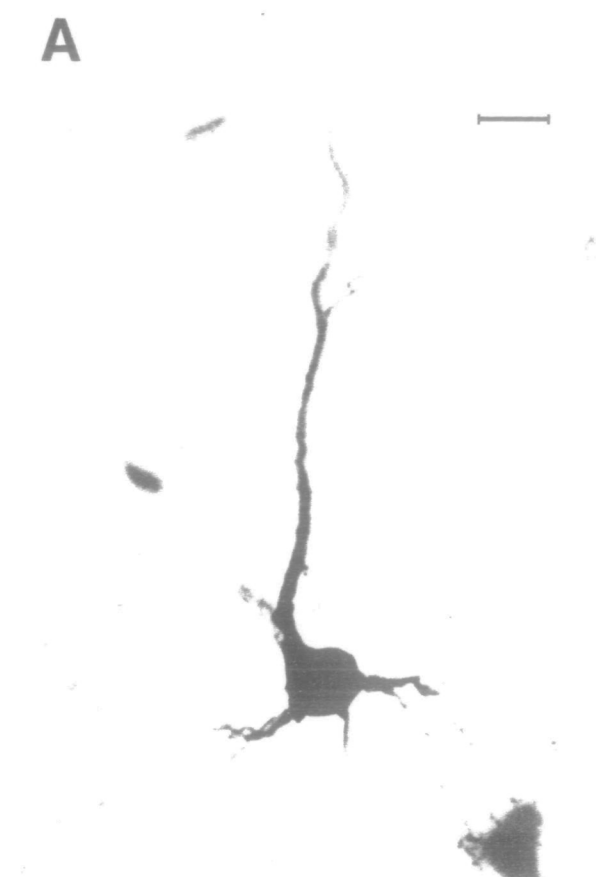
destined for the same layer are born, migrate, and differentiate according to a concurrent inside-to-outside sequence (for review see McConnell, 1988). In this study because the dissociations included cells from all layers, cells of the same class may differ in age by 4 or more days because of their different birthdays. For this reason, there is an approximate 4-day blur across developmental parameters. Neurons of the rat cerebral cortex reach their mature size at around the third postnatal week, i.e., P21 (Parnavelas and Lieberman, 1979; Miller, 1981, 1985; Wolff et al., 1984; Fairen et al., 1986), so we studied all membrane parameters up to at least P21.

## Results

### Identification of Specific Neocortical Cell Types

In the adult rat neocortex the 2 major neuronal types, pyramidal and aspiny stellate cells, display distinctly different morphological and immunohistochemical characteristics, and these distinguishing features (Fig. 1) are retained in many of the neurons dissociated acutely from the neocortex. Figure 1A shows a pyramidal cell that has been retrogradely labeled with HRP while still in a neocortical slice; it is characterized by a single apical dendrite that passes from the apex of the cell body and ascends towards the pial surface. Basilar dendrites radiate from the base of the cell body in a skirt-like fashion. The acutely isolated neocortical neuron (Fig. 1B) displays morphological features that are analogous to the pyramidal neuron (Fig. 1A); furthermore, this cell was immunocytochemically nonreactive for the presence of the enzyme GAD (Oertel et al., 1981). Pyramidal cells lack this enzyme which synthesizes the inhibitory transmitter GABA, whereas the large majority of nonpyramidal cells in the neocortex are GABAergic (i.e.,

**Figure 1.** Two classes of neocortical neurons, identified according to morphological and immunohistochemical criteria, in *in vitro* neocortical brain slices and following acute isolation. *A*, Pyramidal cell in a slice labeled with HRP that was injected into the subcortical white matter and taken up retrogradely by the projecting axons. *B*, Acutely isolated neuron dissociated from rat neocortex. Immunohistochemical staining with anti-GAD was negative for this neuron (i.e., it was non-GABAergic). The dendritic morphology and the absence of GAD staining indicated that it was most likely a pyramidal cell. *C*, Nonpyramidal cell in the neocortex stained positive for the presence of GAD. *D*, Isolated neocortical neuron that showed morphology and GAD staining consistent with that of a nonpyramidal cell. Scale bar is 20 μm in all panels.



inhibitory) and stain positive for the presence of GAD (Ribak, 1978).

In contrast to pyramidal cells, nonpyramidal cells are not morphologically homogeneous (Peters and Kara, 1985); they are characterized by either bipolar or multipolar dendrites rather than a single prominent dendritic process. Figure 1C and 1D show multipolar neurons, positively stained for GAD in a brain slice and in isolation, respectively. In the experiments described here we compared the electrophysiological properties of only those isolated cells whose morphology was similar to that evident in either Figure 1B or 1D (i.e., pyramidal or stellate). Although evidence exists for subclasses within stellate cells, which include, for example, spiny as well as nonspiny stellate cells. The spiny class make up less than 5% of the total and do not stain for GAD (Ribak, 1978). In some experiments, following the recording procedures, the distinctions made between isolated neurons on purely morphological criteria were confirmed using immunocytochemistry for GAD. Subclassification of pyramidal cells has also been made according to laminar position, which also appears to determine their physiological properties (see McCormick et al., 1985). However, because of the difficulty of making this distinction following isolation, our study was restricted to a broader level of comparison.

#### **Action Potential and Repetitive Firing Properties**

The first task in characterizing isolated neocortical neurons was to determine if the same cell-type specific differences in AP shape and repetitive firing properties that distinguish pyramidal from nonpyramidal neurons in neocortical slices (McCormick et al., 1985) are retained in dissociated neurons. A limited number of current clamp recordings revealed that most, but not all, of the differences in firing properties were retained in dissociated neurons. For example, isolated adult neurons with characteristic pyramidal morphology display relatively broad APs (half-width approximately 3 msec at 22°C) with a slow rate of repolarization (Fig. 2A) and no significant spike afterhyperpolarization following a single AP (Fig. 2A). Isolated stellate cells of the same age (P23) display much briefer APs (half-width approximately 1 msec) with a significant postspike afterhyperpolarization (Fig. 2C). In these recordings we held the cells at relatively hyperpolarized potentials (−103 mV and −98 mV, respectively) in order to remove any differences in steady state Na<sup>+</sup> channel inactivation. Similar differences in AP shape and durations have been observed in slice recordings of identified neocortical neuronal classes (McCormick et al., 1985). The differences observed here and those in brain slice studies can be accounted for by the differences in recording temperatures (25°C cf. 34°C) and the Q<sub>10</sub> of AP properties (e.g., Thompson et al., 1985).

Both cell types demonstrate a progressive decrease in duration of their APs with development. For example, the average duration of APs at their half-amplitude, in pyramidal cells at P30 is nearly one-tenth of that of APs in pyramidal cells at E18 ( $1 \pm 0.1$  msec

[P30] cf. with  $8 \pm 0.3$  msec [E18], mean  $\pm$  SD estimated from 10 APs at each age). A similar developmental change in AP kinetics has been reported in studies of pyramidal cells in neocortical slices (McCormick and Prince, 1987). Nonpyramidal cells show an even larger reduction in AP duration ( $5 \pm 0.2$  msec [E18] versus  $0.3 \pm 0.06$  msec [P30]) so that the cell-specific differences in this AP parameter were more pronounced in adult neurons (i.e.,  $P/NP = 1/0.3 = 3.33$ ) compared with embryonic neurons ( $P/NP = 8/5 = 1.6$ ). This developmental change reflects the relatively late postnatal development of K<sup>+</sup> channels that are important in AP repolarization (see below).

The isolated pyramidal and nonpyramidal neurons characterized in Figure 2A,C also displayed differences in their repetitive firing properties in response to constant current stimulation (Fig. 2B,D). To measure these differences, the amplitude of long duration, constant current pulses (not shown) was initially adjusted to activate a single AP in each cell (top traces, Fig. 2B,D) and the depolarization was then increased progressively to produce repetitive firing. Isolated nonpyramidal cells fired at high, sustained frequencies with no signs of adaptation or reduction in AP amplitude even with the strongest depolarization (bottom trace, Fig. 2D). In comparison, isolated pyramidal cells showed a smaller increase in spike firing frequency with increasing depolarization (middle trace, Fig. 2B), and with strong depolarization there was a progressive reduction in spike amplitude until complete AP block occurred (lower trace, Fig. 2B).

In general, it was found that repetitive firing was more difficult to evoke in isolated embryonic and neonatal neurons because of the AP block that occurred soon after the first evoked AP (data not shown). This most likely reflects the lower density of Na<sup>+</sup> channels in immature neurons (see below), which makes them more sensitive to the accumulative effects of depolarization dependent Na<sup>+</sup> current inactivation.

#### **Sodium Conductance**

At the earliest embryonic stage (E17) from which isolated neurons were studied, both classes of cells displayed inward Na<sup>+</sup> currents (Fig. 3A) that could be completely blocked by 200 nM tetrodotoxin (TTX; not shown). At no developmental stage in this study was a TTX-insensitive Na<sup>+</sup> current detected. Both embryonic cell types displayed equal densities of Na<sup>+</sup> current following correction for membrane area (Fig. 3B) and in both cells with increasing age there was a progressive increase in the size of the TTX-sensitive Na<sup>+</sup> current. Although pyramidal and nonpyramidal cells dissociated from neonates of the same age (up to P7) also displayed the same Na<sup>+</sup> current density (Fig. 3B), at later ages between P7 and P20 pyramidal cells showed a higher rate of increase in Na<sup>+</sup> current compared with nonpyramidal cells. This is indicated in the curves of Figure 3B which have been normalized with respect to membrane area. As a result, mature pyramidal cells display almost twice the Na<sup>+</sup> current density when compared with mature nonpyramidal cells.

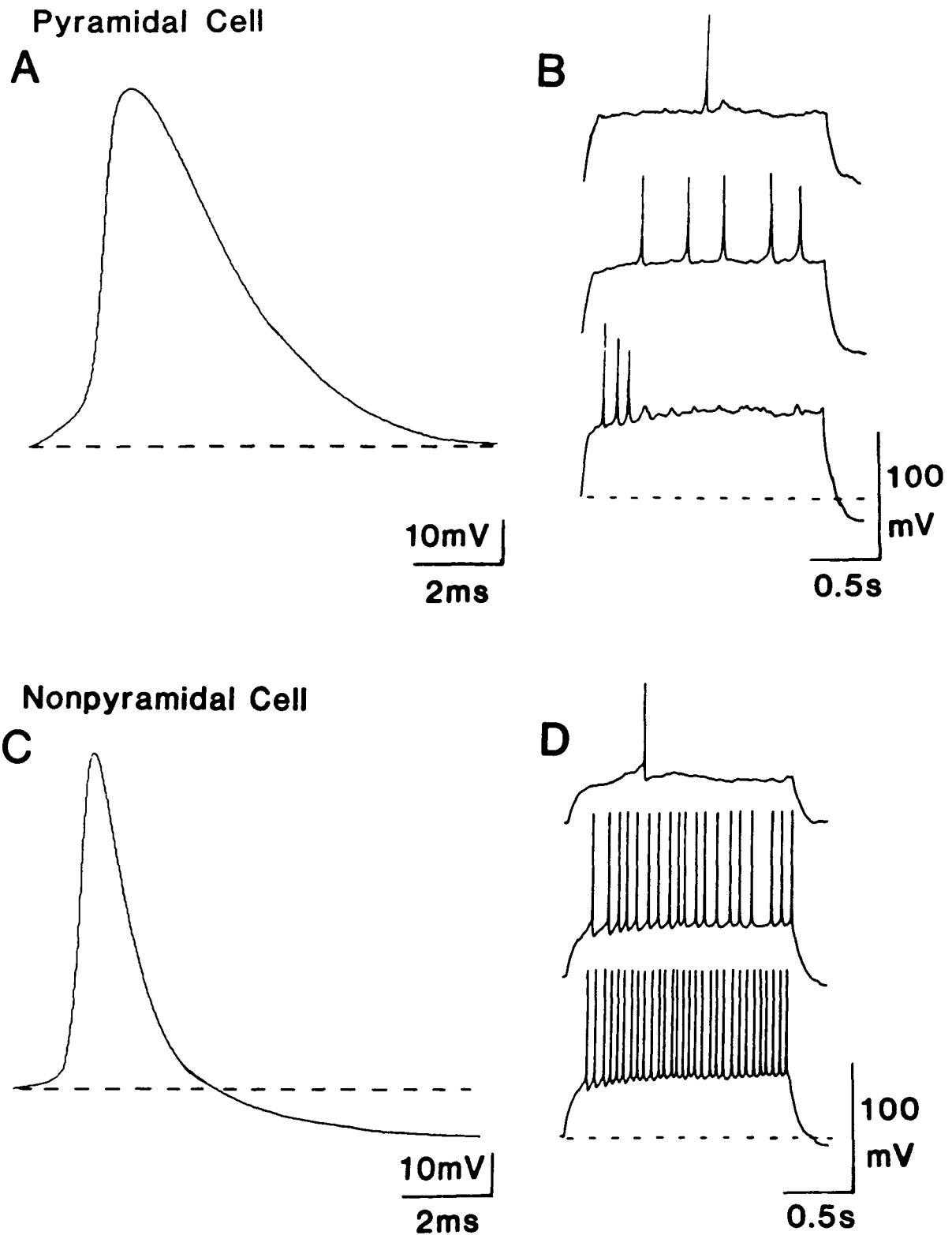
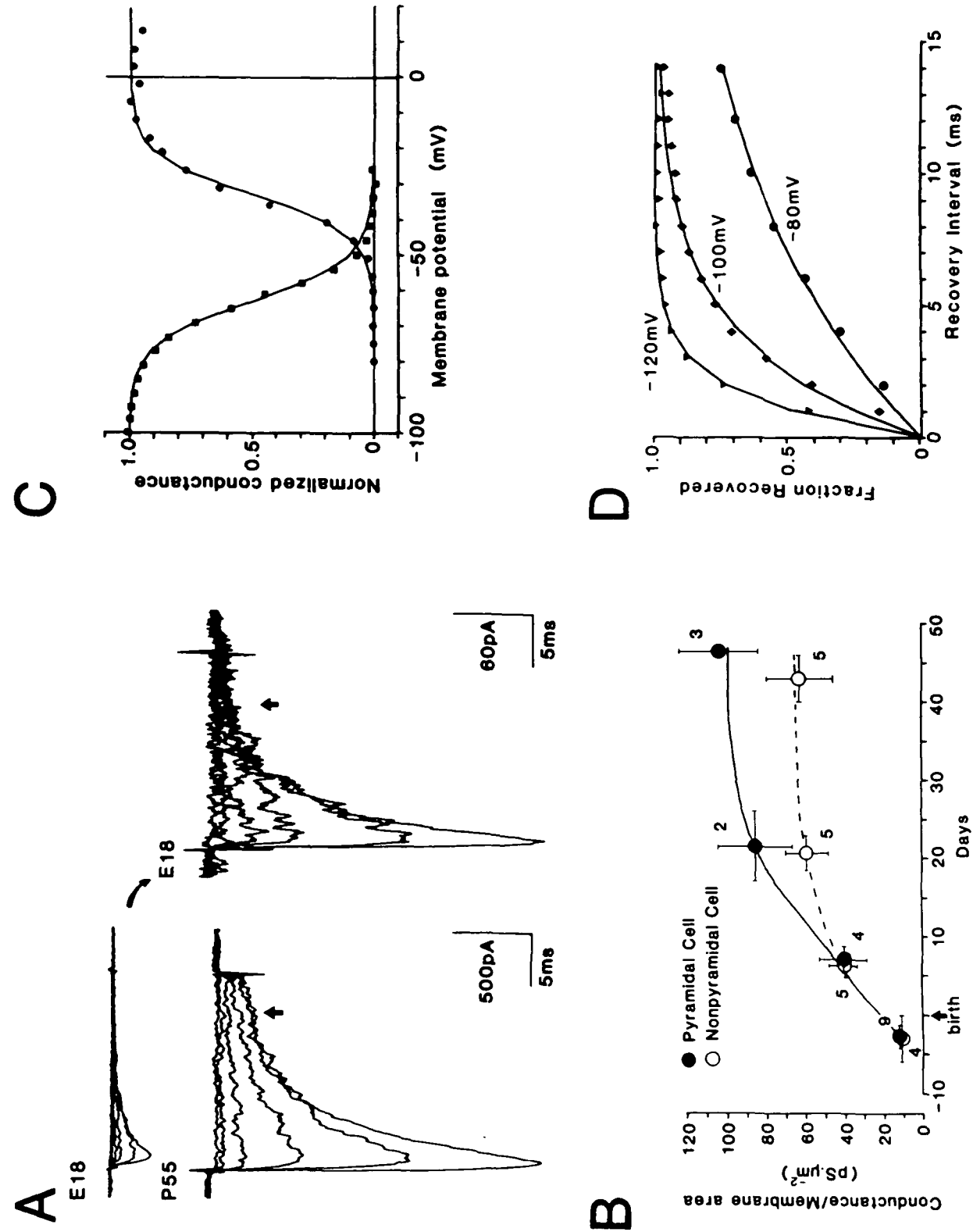


**Figure 2.** Different AP waveforms and repetitive firing properties evident in the 2 morphologically defined classes of isolated neocortical neurons. *A*, Pyramidal cell, P23. Left hand panel, current clamp recording of AP in response to current stimulation. This neuron had an input resistance of approximately 900 M $\Omega$  and a current of 50 pA was required to depolarize the cell to threshold. The AP waveform shows a relatively slow rate of repolarization and an absence of a spike afterhyperpolarization. The *dotted line* represents the base of the AP. Holding potential = -103 mV, AP height = 78 mV, half-width = 2.9 msec. *B*, Right hand panel, responses of the same neuron in *A* to 2-sec-duration constant current depolarizations of increasing intensity (top to bottom). The top trace shows a single AP in response to a near threshold stimulation. With progressively increasing current steps (beginning at 40 pA with steps of 10 pA, traces not shown), repetitive firing was produced (middle trace). However, after the initial AP, subsequent APs were progressively reduced in amplitude until there was complete blockage for the remainder of the pulse (bottom trace). *C*, Nonpyramidal cell of the same age (i.e., P23). This cell had an input resistance of 1200 M $\Omega$  and a current of 40 pA depolarized the cell to threshold, left hand panel. AP showed a relatively rapid rate of repolarization compared to *A*, and an obvious spike afterhyperpolarization. Holding potential = -98 mV, AP height = 75 mV, half-width = 1.1 msec, right hand panel. *D*, Similar protocol as in *B*, this neuron demonstrated higher rates of firing to increasing depolarizations, with no evidence of spike frequency adaptation. External solution was E, and the internal solution was I<sub>1</sub>. Temperature 22–24°C.



Despite the large increase in current amplitude that occurs during development, the voltage dependence of Na<sup>+</sup> current activation does not change. This is illustrated in Figure 3A where the E18 Na<sup>+</sup> peak current shown in the upper trace has been normalized to the same amplitude as the P55 peak current (Fig. 3A, lower right trace) and indicates that the grading in activation is the same in both cases. We have reported previously in detail (Huguenard et al., 1988) that the Hodgkin-Huxley parameters describing the voltage-dependence of activation, steady-state inactivation (Fig. 3C), and recovery from inactivation (Fig. 3D) display no significant variations either as a function of cell type or developmental age. However, there is a developmental change in inactivation kinetics that is evident in both cell types (Huguenard et al., 1988). This is indicated by the residual Na<sup>+</sup> current that remains at the end of the 15-msec pulse in the P55 neuron but which is absent in the E18 neuron (i.e., compare current levels at the *arrows* in Fig 3A). In embryonic neurons Na<sup>+</sup> currents decayed with a single, fast voltage-dependent exponential (time constant of decay 3–1 msec over the range –50 to –30 mV) consistent with the Hodgkin-Huxley model (Hodgkin and Huxley, 1952). By contrast, in the mature neuron, complete decay took approximately 10 times longer and was best fitted with 2 exponentials with fast (3–1 msec) and slow (30–10 msec) time constants. The changes in kinetics were not caused by increased series resistance error due to larger amplitude Na<sup>+</sup> currents because various procedures used to reduce Na<sup>+</sup> current such as reduced extracellular Na<sup>+</sup>, more positive holding potential, and low concentrations of TTX, did not alter inactivation kinetics (Huguenard et al., 1988). The difference is also unlikely to reflect an increased inability to space clamp the more distal processes of more mature cells. The nature of the dissociation procedure results in mature cells having more truncated processes than embryonic or neonatal cells. For example, we actually see a decrease in total membrane area with increasing developmental age. Finally, single Na<sup>+</sup> channel current recordings from mature neurons indicated similar inactivation kinetics in the ensemble averages as observed in macroscopic recordings (Huguenard et al., 1988).

### Potassium Conductance

Figure 4 summarizes the cell-type specific differences and developmental changes in K<sup>+</sup> currents seen in

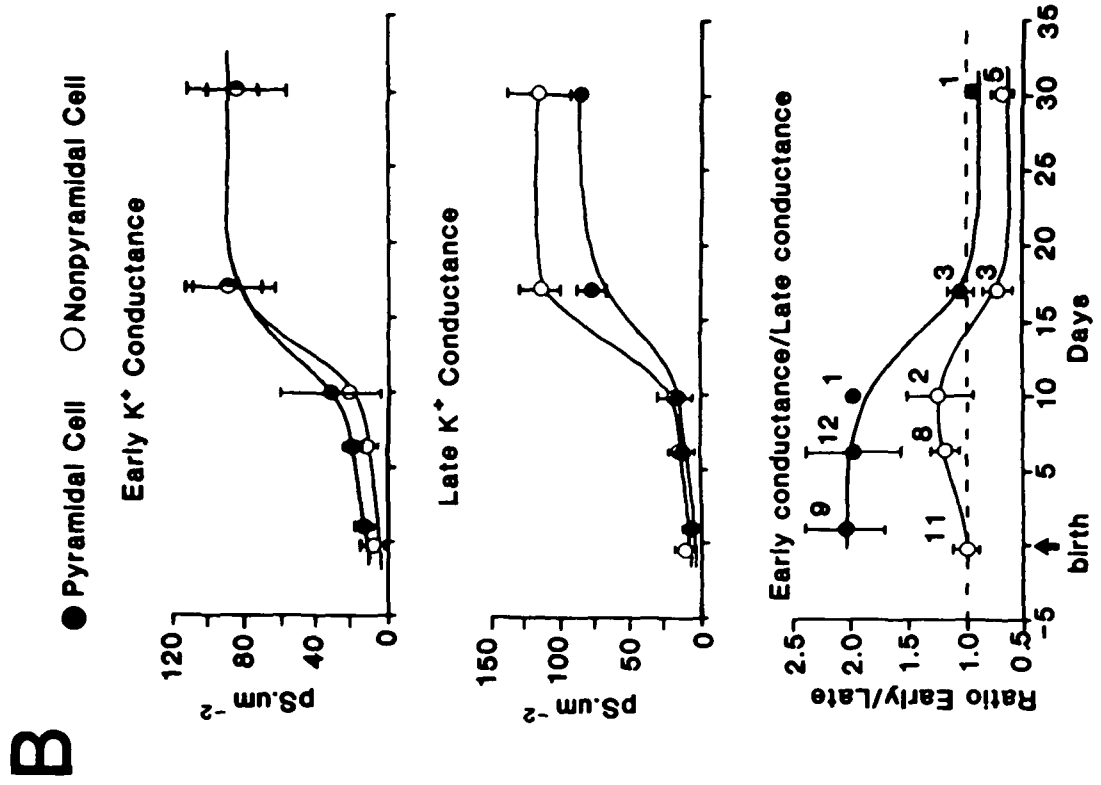
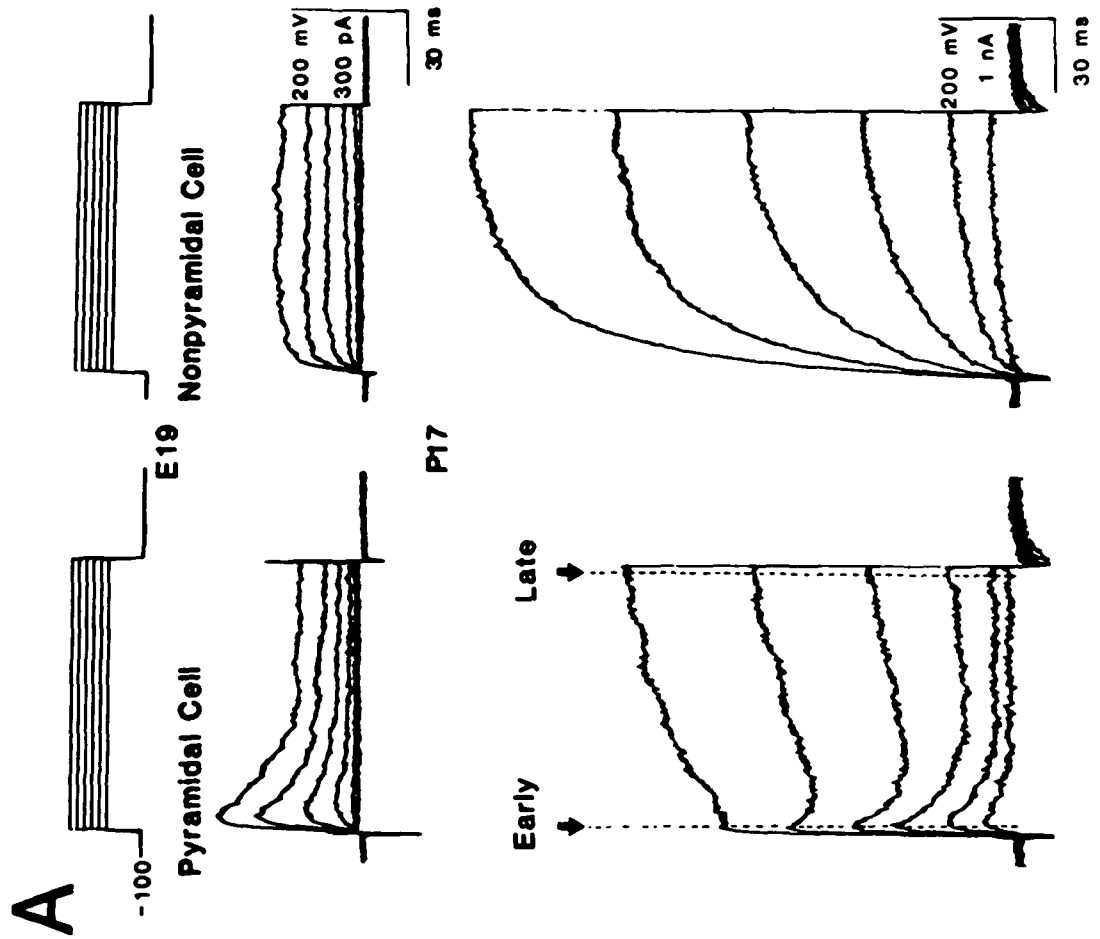
neocortical neurons with external and internal solutions (see Table 1) that minimized the contribution of Ca<sup>2+</sup>-activated K<sup>+</sup> currents, which were not studied here. At very young ages, for example E19 (Fig. 4A, top current traces), K<sup>+</sup> currents display distinctly different kinetic features in pyramidal and nonpyramidal cells. In the pyramidal cell, a transient outward current was activated by depolarizing steps of 20–50 mV from rest, whereas in nonpyramidal cells of the same age, only a noninactivating (sustained) outward current was evident. In more mature neurons (>P17), the clear distinction in kinetics was somewhat concealed because pyramidal cells developed a “new” or “late-developing” sustained current that superimposed on the transient current to produce complex current waveforms (bottom current traces, Fig. 4A; note change in scale). In more mature nonpyramidal cells, a transient current did not appear, but the sustained current became larger.

In order to quantify the observed cell-type specific developmental changes, current amplitudes were measured 5 msec (early) and 95 msec (late) subsequent to initiating voltage steps (Fig. 4A). The normalized early and late currents are plotted in the top and middle graphs of Figure 4B, respectively, and the bottom graph is a representation of the ratio of early to late conductance as a function of age. Both early and late K<sup>+</sup> conductance exhibited a gradual increase up to P10 and then a steeper increase to P20; beyond this age a constant level was attained (Fig. 4B, top and middle graphs). While cells of both types appear to reach the same mature level (i.e., after P20) of early K<sup>+</sup> conductance, despite the absence of the transient current in nonpyramidal cells, this occurred because nonpyramidal cells demonstrate a *higher* final density of the late K<sup>+</sup> conductance, indicating a larger sustained current. The graph comparing ratios of early to late currents illustrates the differences in developmental changes in early and late K<sup>+</sup> currents in the 2 cell types (bottom graph, Fig. 4B).

The differences in voltage dependencies of Hodgkin-Huxley parameters of activation and inactivation of the transient and sustained currents were compared in dissociated neurons of a P1 rat (Fig. 5A), because at this age the 2 currents are selectively expressed, and can be studied independently of one another. The differences (see legend, Fig. 5A) between the transient and sustained current are essentially similar to differences reported previously for the A current and the delayed rectifier, with the A current showing

←

**Figure 3.** Properties of Na<sup>+</sup> currents as a function of cell type and developmental stage. *A*, Differences in current amplitudes and inactivation kinetics as a function of developmental stage, upper left hand trace. Superimposed are Na<sup>+</sup> currents in an embryonic nonpyramidal cell (E18) in response to step voltage commands starting at –60 mV with 6 mV steps. The peak current of the mature (P55) neuron is ~11-fold larger in magnitude when normalized for membrane area. In the lower right hand panel the currents from the embryonic cell have been scaled up in amplitude for purposes of comparison of the activation properties and inactivation kinetics of the Na<sup>+</sup> current. In the mature cell the current slowly inactivates such that at a latency of 15 msec (*left arrow*) a residual current is left, compared to the immature neuron in which the current is nearly completely inactivated (*right arrow*). *B*, Na<sup>+</sup> conductance normalized for membrane area shows a developmental increase over the period of E18 to P45; nonpyramidal cells demonstrated a lower density of Na<sup>+</sup> current especially manifested after day P10. *C*, Steady-state inactivation (*squares*) and peak activation (*circles*) curves for the peak Na<sup>+</sup> current, day E18 pyramidal neuron. The current was half-inactivated at a potential of –65 mV with a voltage dependence of 6.1 mV per e-fold change in peak Na<sup>+</sup> current. Half-activation occurred at –35 mV with a slope of 5.2 mV/e-fold. *D*, Plots of time course of recovery from inactivation of Na<sup>+</sup> currents, day P2 pyramidal cell. Recovery curves were well fitted with single exponentials with time constants of (–120) 2.5, (–100) 4.0, and (–80) 12 msec. External solution, E<sub>2</sub> and internal solution, I<sub>2</sub>. The exponential curves were fitted according to the conventional Hodgkin-Huxley model (Hodgkin and Huxley, 1952).



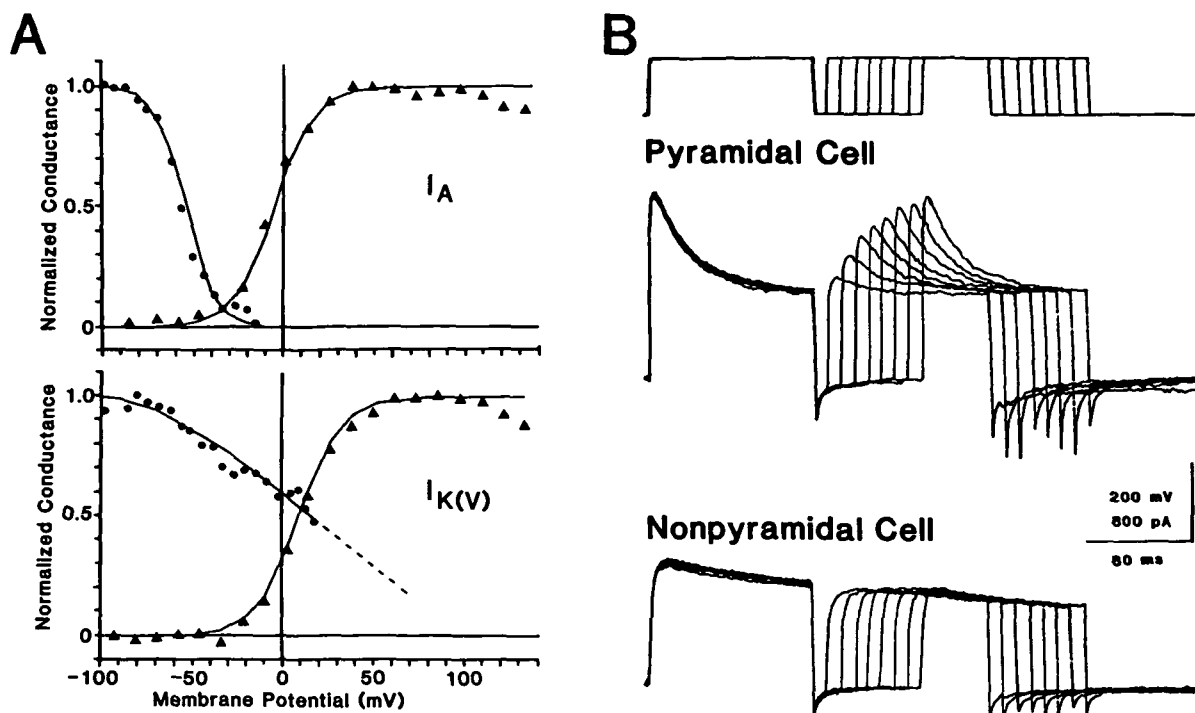


**Figure 5.** *A*, Activation and steady-state inactivation of the transient current ( $I_A$ ) and the noninactivating current ( $I_{K(V)}$ ) measured in 2 different neurons that selectively express one of the currents. *Upper panel*, steady state inactivation (circles) and activation (triangles) curves for peak  $I_A$ . Day P1 pyramidal neuron. The current was half-inactivated at a potential of  $-61$  mV with a voltage dependence of  $6.1$  mV per e-fold change in peak  $K^+$  current. Half-activation occurred at  $-31$  mV with a slope of  $5.2$  mV/e-fold. *Lower panel*, steady state inactivation (circles) and activation (triangles) curves for the peak delayed  $K^+$  current ( $I_{K(V)}$ ). Day P1 nonpyramidal cell. The current was half-inactivated at a potential of  $18$  mV with a voltage dependence of  $40$  mV per e-fold change in peak  $K^+$  current. Half-activation occurred at  $10$  mV with a slope of  $5.2$  mV/e-fold. *B*, Illustration of the differences in the inactivation and recovery from inactivation of A currents and the noninactivating currents recorded in a pyramidal cell (*top trace*) and nonpyramidal cell (*bottom trace*). Both cells were held at  $-100$  mV and both came from the same P7 rat dissociation. The recovery was fit with a single exponential (not shown) with a time constant of  $35$  msec. Same solutions as in Figure 4.

activation and steady-state inactivation at relatively less depolarized potentials and the delayed K current showing only incomplete inactivation at positive voltages (Adams et al., 1980; Adams and Galvan, 1984).

A final distinction between the 2 currents exists in their rates of recovery from inactivation, which is illustrated in 2 neurons isolated from a P7 rat (Fig. 5*B*). In pyramidal cells the transient current shows a relatively rapid recovery from full inactivation (e.g., the time constant of recovery was approximately  $40$  msec; top trace, Fig. 5*B*), whereas the sustained current in nonpyramidal cells requires several seconds for recovery from its incomplete inactivation.

#### Calcium Conductance

Under ionic conditions that block  $Na^+$  and  $K^+$  currents (see Table 1),  $Ca^{2+}$  currents were recorded in both classes of neocortical neurons. This is illustrated in

Figure 6, which shows  $Ca^{2+}$  currents recorded from pyramidal and nonpyramidal cells of the same age (P11). Both cell types displayed evidence of 2 classes of  $Ca^{2+}$  currents, the characteristics of which are illustrated in Figure 7. At the youngest age studied (E19), the  $Ca^{2+}$  current in both cell types had properties indicative of a class of  $Ca^{2+}$  channel referred to as the high threshold, noninactivating or L-type  $Ca^{2+}$  channel (e.g., see Carbone and Lux, 1984; Nowycky et al., 1985). It was activated at relatively depolarized potentials (with a half-maximal activation at  $-15$  mV) and displayed little steady-state or time-dependent inactivation (Fig. 7*B*). This  $Ca^{2+}$  current increased in size with developmental age in both cell types, there occurring approximately a 3-fold increase in peak L-type  $Ca^{2+}$  conductance ( $7 \pm 3$  pS/ $\mu m^2$  to  $22 \pm 5$  pS/ $\mu m^2$ , mean  $\pm$  SD, estimated from 4 cells of each type at each age) between the ages of  $\sim$ P1 and  $\sim$ P27.

←

**Figure 4.** Potassium currents obtained in neocortical neurons of different cell types at different developmental ages. *A*, Upper traces. Outward currents obtained in pyramidal and nonpyramidal neurons at stage E19. Voltage steps ranged  $-60$  to  $-25$  mV from a holding potential of  $-100$  mV. The pyramidal cell demonstrates a current that almost completely inactivates whereas in the nonpyramidal cell the outward current does not inactivate. Lower traces; currents corresponding to the same voltage steps as in the upper traces, but at developmental stage P17. The early (5 msec after the pulse) and late currents (95 msec after the pulse) are both larger in magnitude (note change in scale), but the late current has shown a relatively larger developmental increase compared with the early current such that the superimposed late current tends to obscure evidence of the transient current. *B*,  $K^+$  current density at different latencies as a function of developmental age. *Upper panel*, normalized  $K^+$  current density from the slope of the maximum I-V curve of the 5-msec latency current in both cell types. Nonpyramidal neurons demonstrate slightly smaller early  $K^+$  currents, especially at early developmental stages. *Middle panel*,  $K^+$  current density at 95 msec latency. Pyramidal neurons have a lower late  $K^+$  current density at every developmental stage than nonpyramidal neurons. *Lower panel*, ratio of early to late current density. Pyramidal cells at early development show larger disparity between early and late than the nonpyramidal cells. External solution was  $E_3$  and internal solution was  $I_3$ .

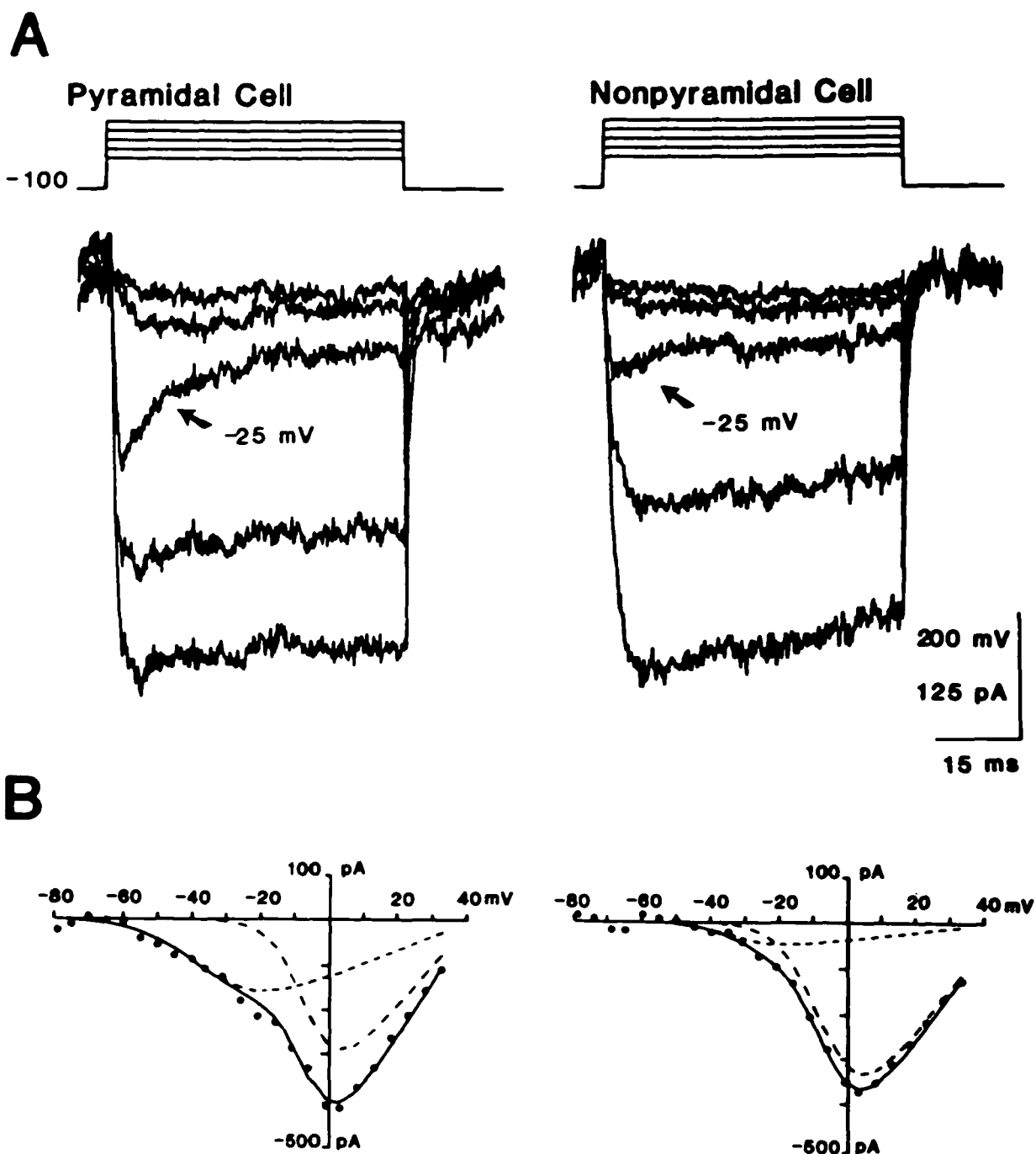


**Figure 6.** Calcium currents recorded from different cell types of the same age (P11). *A*, Calcium currents recorded from a pyramidal and nonpyramidal neuron during 50-msec steps to voltages in the range of  $-50$  to  $-15$  mV. Each cell type displays a noninactivating current of the same amplitude but the transient current (see *arrows* for currents recorded at  $-25$  mV in each cell type) is larger in the pyramidal cell. *B*, I-V relationships for the 2 neurons in *A*. The 2 *dashed curves* within each I-V represent the best fit function for a 2 component voltage sensitive activation. The values for half-maximal activation of the low and high threshold currents in the pyramidal cell were  $-70$  mV and  $-10$  mV, with slopes of 12 mV and 5 mV per e-fold and  $g_{Ca^{2+}}$  values of 20 and 40  $\text{pS}/\mu\text{m}^2$ , respectively. In the nonpyramidal cell, the values for low and high threshold currents were  $-65$  mV and  $-10$  mV, with slopes of 12 mV and 5 mV per e-fold, and  $g_{Ca^{2+}}$  values of 5 and 60  $\text{pS}/\mu\text{m}^2$ , respectively. External solution  $E_c$ , internal solution  $I_i$ .

In neurons from animals P4 and older, an additional  $\text{Ca}^{2+}$  current with quite different properties, was also resolved (most easily in pyramidal cells) and this has features (Fig. 7*A*) similar to a class of  $\text{Ca}^{2+}$  channel referred to as the low threshold, transient or T-type  $\text{Ca}^{2+}$  channel (e.g., see Carbone and Lux, 1984; Nowycky et al., 1985). It was activated at less depolarized potentials (with a half-activation at  $-30$  mV) and

showed both time-dependent and steady-state inactivation at relatively less depolarized potentials (see Fig. 7 legend). We were unable to detect a current with these characteristics in neurons from either a P1 or P2 dissociation. The occurrence of this current at older ages ( $>P3$ ) varied in both cell types but was always more prominent in pyramidal cells compared with nonpyramidal cells of the same age.

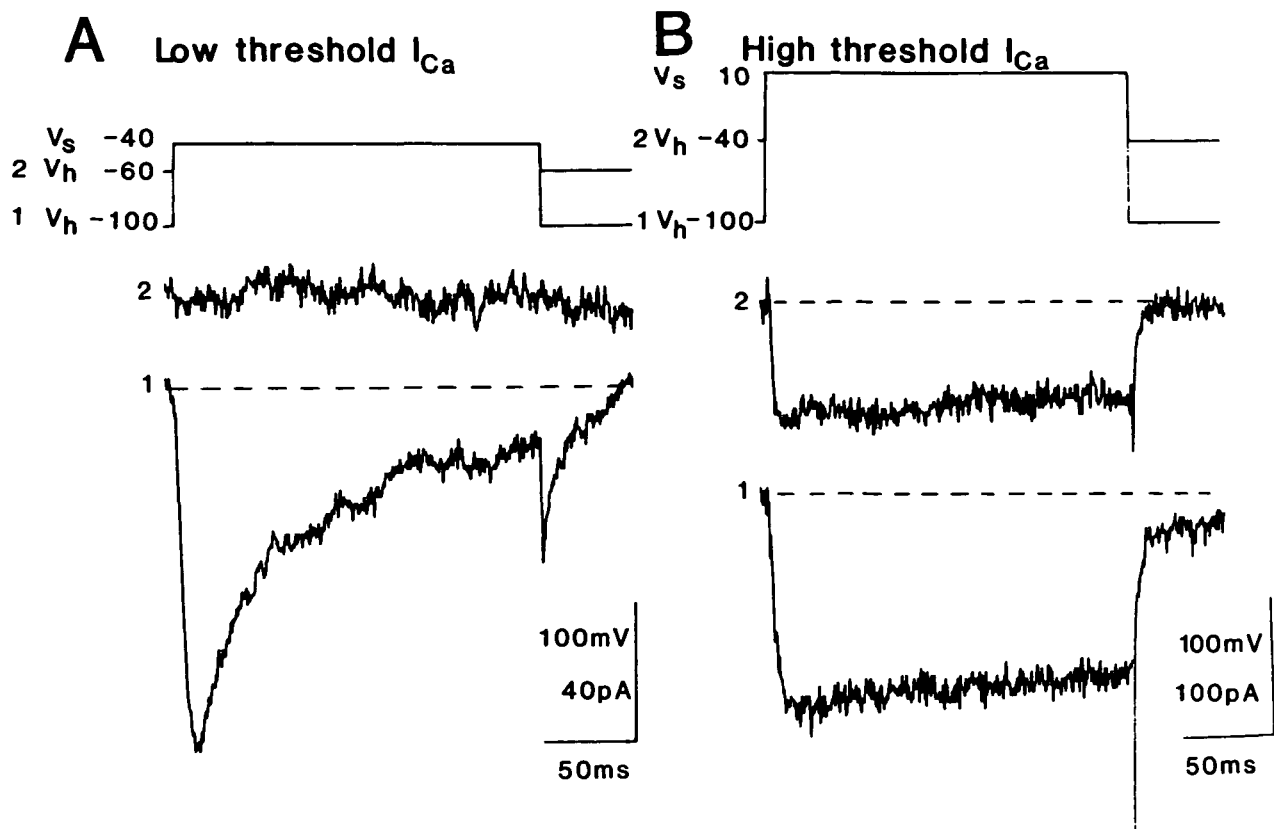


**Figure 7.** Properties of the transient and noninactivating  $Ca^{2+}$  currents measured in the same pyramidal cell (P27). *A*, Transient  $Ca^{2+}$  current obtained with depolarizations to  $-40$  mV. With reduction in the holding potential from  $-100$  mV to  $-60$  mV, the transient  $Ca^{2+}$  current and the associated slow tail current were completely blocked. *B*, Noninactivating  $Ca^{2+}$  current in same neuron as in *A*, obtained with depolarizations to  $+10$  mV. When the holding potential was reduced from  $-100$  mV to  $-40$  mV, there was only a small reduction in the noninactivating current (partly due to rapid washout of this current) but the slow component of the tail current was blocked (the fast portion was truncated here due to space limitations). Same solutions as in Figure 6.

Reexamination of Figure 6 illustrates the typical cell-type specific difference in expression of the T- and L-class  $Ca^{2+}$  currents. In the pyramidal cell a transient inward current is evident at  $-27$  mV, whereas in the nonpyramidal cell at the same potential the transient current is barely detectable, even though the noninactivating currents are of similar size in the 2 cells. Figure 6*B* shows the current-voltage relationships for the currents in Figure 6*A*; the broken curves were calculated from Boltzmann distributions assuming independently activated current components. The calculated ratio of peak T-current component to L-current component was 0.5 for the pyramidal cell compared with 0.08 for the nonpyramidal cell, both at P11. Similar ratios of T/L currents were observed in cells from 2 other dissociations from P12 and P13 rats ( $0.6 \pm 0.1$  [P],  $0.09 \pm 0.01$  [NP]). However, our  $Ca^{2+}$  current data on older cells were too variable to determine if there is a late postnatal divergence in cell-specific densities of either the T- or L-type  $Ca^{2+}$  channels, as was observed for  $Na^+$  and  $K^+$  channels.

### Discussion

The results of this study provide some biophysical information on the mechanisms that underlie certain differences in AP shape and repetitive firing properties observed in different classes of neocortical neu-

rons (McCormick et al., 1985). As in the previous brain slice study we have focused our attention on differences between the 2 major, and most easily distinguishable types of neurons in the cerebral cortex, the pyramidal and GABAergic nonpyramidal (aspiny stellate) cells. One of the most distinctive differences reported between the 2 cell types at the level of the single AP, is the difference in AP duration. Whereas pyramidal cells have a relatively broad AP, the aspiny stellate cells have a very brief AP. This study indicates that the relatively higher ratio of delayed  $K^+$  current density to the  $Na^+$  current density, expressed by the stellate cell is the main factor contributing to its characteristic AP shape. The relative dominance of delayed  $K^+$  in the stellate cell contributes to both its faster repolarization and more pronounced spike afterhyperpolarization.

It is interesting, given the diversity of different subclasses of  $Na^+$  and  $K^+$  channels that have been indicated by recent DNA and cloning studies (Trimmer and Agnew, 1989; Stühmer et al., 1989), that we were unable to detect significant cell-type specific differences in other characteristics of the  $Na^+$  and delayed  $K^+$  currents. It would appear that both neocortical cell types express identical or functionally similar  $Na^+$  and delayed  $K^+$  channels, and differ only in the mature channel densities they express. Since both

types show a progressive increase in current density as the cells mature, there must be signals that regulate the final channel density reached in each cell, in an apparent reciprocal manner. Whether the signal(s) reflect differences within intrinsic genetic programs or environmental experiences remains to be determined. However, one possible clue to their nature is indicated by the observation that divergence, in at least these channel densities, becomes evident only relatively late postnatally (i.e., >P10) when neocortical neurons are undergoing synaptogenesis. Consistent with the observation of delayed appearance of the cell-type specific changes in K<sup>+</sup> current density, we observe little differences in AP durations in pyramidal and nonpyramidal cells at earlier stages of development.

Whatever the nature of the mechanism that leads to neuronal functional divergence, it is clear that the differences in AP shape have important consequences for the functional properties of the neurons. The brief AP duration and spike afterhyperpolarization displayed by stellate cells will reduce the accumulation of depolarization-dependent Na<sup>+</sup> channel inactivation, which would otherwise reduce AP amplitude during long trains of high frequency APs; it will also reduce the amount of Ca<sup>2+</sup> flowing into the cell via depolarization activated Ca<sup>2+</sup> channels. Consequently, Ca<sup>2+</sup>-activated K<sup>+</sup> channels that might, under other conditions, hyperpolarize the cell and reduce firing frequency, will be less activated in the stellate cell. Pyramidal cells on the other hand appear not to require the same adaptations for high frequency tonic firing, presumably because, as discussed below, they serve a different role in neocortical circuit function.

Pyramidal cells, compared with stellate cells, express more strongly both the A current and the T-type Ca<sup>2+</sup> current. Both these subthreshold currents provide the pyramidal cell with different mechanisms for voltage-dependent modulation of firing patterns; the A current provides a way of introducing delays and slowing the frequency of repetitive discharges (Connor and Stevens, 1971); the T-type Ca<sup>2+</sup> current enables high-frequency phasic activity characterized by initial bursts of APs on a depolarizing pedestal (Llinás and Jahnsen, 1982). In combination, the 2 currents can provide a mechanism for supporting rhythmic burst firing (Steriade and Llinás, 1988). The selective expression of the threshold currents in the pyramidal cell is consistent with a more integrative role in sculpturing its final output. In contrast, the relative absence of subthreshold currents in inhibitory stellate cells is consistent with their primary role being to provide a reliable transformation of excitatory input into inhibitory output, with apparently less need for modulation.

In conclusion, the present study indicates that the different firing properties of the main classes of neocortical neurons are determined by differences in expression of at least 4 types of voltage-gated channels. For some channels, the differences occur only in the relative density expressed late postnatally (>P10). For other channels (e.g., the A-current channel) there

is an apparent all-or-none difference in expression that is evident even in embryonic neurons. This study represents only a first step in characterizing all of the subclasses of channels that may be expressed by neocortical neurons. Clearly, additional molecular biological approaches, in combination with electrophysiological ones, will be required to understand fully the developmental mechanisms that underlie cell-type specific neuronal membrane properties.

## Notes

We thank Elizabeth Enayati for her technical assistance in preparing the cells and Jay Kadis for his assistance and advice. We also thank Barbara Seely for typing the manuscript. Supported by NIH grants NS 064477, NS 12151, the Morris research fund (DAP) and NSF grant, and the Klingenstein fund (OPH).

Address correspondence and reprint requests to Dr. Owen P. Hamill, Section of Neurobiology and Behavior, Seeley G. Mudd Hall, Cornell University, Ithaca, NY 14853.

## References

- Adams PR, Galvan M (1984) Voltage-dependent currents of vertebrate neurons and their role in membrane excitability. *Adv Neurol* 44:137-170.
- Adams DJ, Smith SJ, Thompson SH (1980) Ionic currents in molluscan soma. *Ann Rev Neurosci* 3:141-167.
- Berry M, Rogers AW (1965) The migration of neuroblasts in the developing cerebral cortex. *J Anat* 99:691-709.
- Carbone E, Lux HD (1984) A low voltage-activated, fully inactivating Ca channel in vertebrate sensory neurones. *Nature* 310:501-502.
- Connor JA, Stevens CF (1971) Prediction of repetitive firing behavior from voltage clamp data on an isolated neuron soma. *J Physiol (Lond)* 213:31-53.
- Fairen A, Cobas A, Fonseca M (1986) Times of generation of glutamic acid decarboxylase. Immunoreactive neurons in mouse somatosensory cortex. *J Comp Neurol* 251:67-83.
- Gilbert CD, Wiesel TN (1979) Morphology and intracortical projection of functionally characterized neurones in the cat visual cortex. *Nature* 280:120-126.
- Hamill OP, Marty A, Neher E, Sakmann B, Sigworth FJ (1981) Improved patch-clamp techniques for high-resolution current recording from cells and cell-free membrane patches. *Pflügers Arch* 391:85-100.
- Hicks SP, D'Amato CJ (1968) Cell migration to the isocortex in the rat. *Anat Rec* 160:619-634.
- Hodgkin AL, Huxley AF (1952) A quantitative description of membrane current and its application to conduction and excitation in nerve. *J Physiol* 117:500-544.
- Hubel DH, Wiesel TN (1962) Receptive fields, binocular interaction and functional architecture in the cat's visual cortex. *J Physiol* 160:106-154.
- Huguenard JR, Hamill OP, Prince DA (1988) Developmental changes in Na<sup>+</sup> conductances in rat neocortical neurons: appearance of a slowly inactivating component. *J Neurophysiol* 59:778-795.
- Kay AR, Wong RKS (1986) Isolation of neurons suitable for patch-clamping from adult mammalian central nervous systems. *J Neurosci Meth* 16:227-238.
- Kelly JP, Van Essen DC (1974) Cell structure and function in the visual cortex of the cat. *J Physiol* 238:515-547.
- Llinás R, Jahnsen H (1982) Electrophysiology of mammalian thalamic neurons *in vitro*. *Nature* 297:406-408.
- McConnell SK (1988) Development and decision making in the mammalian cerebral cortex. *Brain Research Reviews* 13:1-23.
- McCormick DA, Prince DA (1987) Post-natal development of electrophysiological properties of rat cerebral cortical pyramidal neurons. *J Physiol* 393:743-762.
- McCormick DA, Connors BW, Lighthall JW, Prince DA (1985)

- Comparative electrophysiology of pyramidal and sparsely spiny stellate neurons of the neocortex. *J Neurophysiol* 54:782-806.
- Mesulam M-M (1982) Tracing neural connections with horseradish peroxidase. New York: John Wiley and Sons.
- Miller MW (1981) Maturation of rat visual cortex. I. A quantitative study of Golgi-impregnated pyramidal neurons. *J Neurocytol* 10:859-878.
- Miller MW (1985) Cogeneration of retrogradely labeled cortico cortical projection and GABA-immunoreactive local circuit neurons in cerebral cortex. *Dev Brain Res* 23:187-192.
- Mountcastle VB (1957) Modality and topographic properties of single neurons of cat's somatic sensory cortex. *J Neurophysiol* 20:408-434.
- Nowycky MC, Fox AP, Tsien RW (1985) Three types of neuronal calcium channels with different agonist sensitivity. *Nature* 316:440-443.
- Oertel WH, Schmechel DE, Mugnaini E, Tappaz ML, Kopin IJ (1981) Immunocytochemical localization of glutamate decarboxylase in rat cerebellum with a new antiserum. *Neurosci* 6:2715-2735.
- Parnavelas JG, Lieberman AR (1979) An ultrastructural study of the maturation of neuronal somata in the visual cortex of the rat. *Anat Embry* 157:311-328.
- Peters A, Jones EG (1984) Cerebral cortex, Vol 1, Cellular components of the cerebral cortex. New York: Plenum.
- Peters A, Kara DA (1985) The neuronal composition of area 17 of rat visual cortex. II. The nonpyramidal cells. *J Comp Neurol* 234:242-263.
- Ribak CE (1978) Aspinous and sparsely-spinous stellate neurons in the visual cortex of rats contain glutamic acid decarboxylase. *J Neurocytol* 7:461-478.
- Schmitt FO, Worden FG, Adelman G, Dennis SG (1985) The organization of the cerebral cortex, Proceedings of a Neuroscience Research Program Colloquium. Cambridge, MA: MIT Press.
- Shimada M, Langman J (1970) Cell proliferation, migration and differentiation in the cerebral cortex of the golden hamster. *J Comp Neurol* 139:227-244.
- Steriade M, Llinás RR (1988) The functional states of the thalamus and the associated neuronal interplay. *Physiol Rev* 66:649-742.
- Stühmer W, Ruppersberg JP, Schröter KH, Sakmann B, Stocker M, Giese KP, Perschke A, Baumann A, Pongs O (1989) Molecular basis of functional diversity of voltage-gated potassium channels in mammalian brain. *EMBO J* 8:3235-3244.
- Thompson SM, Masukawa LM, Prince DA (1985) Temperature dependence of intrinsic membrane properties and synaptic potentials in hippocampal CA1 neurons *in vitro*. *J Neurosci* 5:817-824.
- Trimmer JS, Agnew WS (1989) Molecular diversity of voltage-sensitive Na channels. *Rev Physiol* 51:401-418.
- Wolf JR, Battcher H, Zetzche T, Oertel WH, Chronwall BB (1984) Development of GABAergic neurons in rat visual cortex as identified by glutamate decarboxylase-like immunoreactivity. *Neuroscience Letts* 47:207-212.